RSC Advances

ROYAL SOCIETY OF CHEMISTRY

www.rsc.org/advances

Adsorption of Fructose in Sn-BEA Zeolite from Periodic Density Functional Calculations

Gang Yang[a,b,*], Xiong Li[a], Lijun Zhou[a]

[a] College of Resources and Environment *& Chongqing Key Laboratory of Soil Multi-scale Interfacial Process*, Southwest University, Chongqing 400715, China;

[b] Schuit Institute of Catalysis, Eindhoven University of Technology, Eindhoven, 5600MB, the Netherlands.

* To whom correspondence should be addressed:

Email: theobiochem@gmail.com;

Phone: 086-023-68251504; Fax: 086-023-68250444.

Abstract: Fructose is regarded as a key intermediate for transformation of cellulosic biomass to downstream products. In gas phase, D-fructofuranose conformers that predominate in biochemically relevant polysaccharides are strongly disfavoured, and the condition improves slightly by inclusion of bulk solvent effects. The various O sites in four selected fructose conformers are accessible to the Sn Lewis acidic site of Sn-BEA zeolite except five cases mainly as a result of steric hindrances from the adjacent groups. The adsorption energies of fructose in Sn-BEA zeolite are calculated within -73.3 ~ -161.5 kJ/mol that may differ substantially for the various conformers and various O sites. D-fructofuranose rather than D-fructopyranose conformers are significantly preferred in Sn-BEA zeolite and this fundamentally alters the conformational preference of gas phase, as corroborated by the computational relative stabilities ranking as **F4** ≤ **F3** < **F1** < **F2**. Accordingly, D-fructofuranose conformers that predominate in biochemically relevant polysaccharides exist favorably in Sn-BEA zeolite. Dispersion interactions in gas phase can alter the relative stabilities of fructose conformers not more than 5.6 kJ/mol; however, dispersion interactions play a considerably larger role during the interaction with Sn-BEA zeolite that are averaged at -123.8, -123.4, -125.6 and -127.5 kJ/mol for **F1**, **F2**, **F3** and **F4**, respectively.

Keywords: Sn-BEA; adsorption; periodic DFT calculations; relative stability; dispersion interaction

1. Introduction

Cellulosic biomass is a sustainable energy source that has shown great potential to replace the depleting petroleum resources [1, 2]. Currently, the direct transformation of cellulosic sugars (e.g., glucose) to downstream products represents a grand challenge, and a plausible solution is to use fructose as the intermediate product, because fructose can be further converted with high selectivity [3]. Recent studies have demonstrated that Sn-BEA zeolite displays unprecedented catalytic activity for the isomerization of glucose to fructose [4], while a number of related issues, including the adsorption of fructose in Sn-BEA zeolite, remain uncharted.

Fructose in biochemically relevant polysaccharides exists in the furanose form, and hence all previous adsorption and catalytic studies were based on D-fructofuranose [3, 5-13]. The Brønsted-acid catalysis of D-fructofuranose dehydration was demonstrated to be preferential at the O_2H site [14] that ignites a sequence of facile reaction steps towards the production of 5-hydroxymethylfurfural (HMF); instead, activation of D-glucopyranose by Brønsted acids seems to be apparently more difficult, and what adds the difficulty is that those OH sites with relatively higher priority for protonation are inclined to result in humin precursors or reversion products rather than downstream products [3]. Models of different sizes (2-T, 5-T and 46-T clusters as well as periodic model within the framework of density functional theory (*p*-DFT)) were used to study the adsorption of β-D-fructofuranose in H-form ZSM-5 zeolite [15]. It was found that structural parameters of 46-T rather than small clusters (e.g., 2-T and 5-T) are in good agreement with those of *p*-DFT calculations, while all cluster models in combination of B3LYP density functional can not account properly for dispersion effects [16-22], which were assessed by the *p*-DFT calculations to contribute -127.5 kJ/mol to the

adsorption energies. To the best of our knowledge, the adsorption behavior of fructose in Sn-BEA has not yet been reported, albeit the significance is apparent in that fructose plays a pivotal role in the utilization of cellulosic biomass as aforementioned. In this work, adsorption of D-fructofuranose in Sn-BEA zeolite was investigated by use of *p*-DFT calculations, considering both α- and β-conformers as well as all O atoms in these conformers. In addition, contributions of dispersion effects were evaluated for all relating adsorption processes.

Recently, Cocinero et al. [23] observed that free fructose is conformationally locked as D-pyranose instead of D-furanose. Which will be preferred when adsorbed within Sn-BEA zeolite, D-fructopyranose or D-fructofuranose? It may alter the reaction paths of isomerization reaction and further the product distributions, thus representing a topic of interest. To address this point, *p*-DFT calculations were also performed to investigate the adsorption of D-fructopyranose in Sn-BEA zeolite, with consideration of both α- and β-conformers as well as all O atoms in these conformers. Likewise, dispersion effects were evaluated for all relating adsorption processes, which were then compared with the results of D-fructofuranose conformers.

2. Computational Section

2.1. Fructose conformers

In agreement with previous works [6-13, 15], the lowest-energy α- and β-conformers were the choice for the present investigation, resulting in a total of four conformers for fructose. As shown in Figure 1, two conformers are presented as D-furanose that is the predominant form in biochemically relevant polysaccharides while the other two as D-pyranose that is the predominant form in gas phase [23, 24]. Structural optimizations

were optimized at the MP2/6-31+G(d,p) level of theory followed by frequency calculations verifying that these stationary points are all energy minima [25]. Unless otherwise noted, all structural parameters and relative energies in gas phase were reported at this level.

To testify the validity of other functionals for describing dispersion interactions, the gas-phase fructose conformers were also investigated by HF/6-31+G(d,p), B3LYP/6-31+G(d,p) and M06L/6-31+G(d,p) [26, 27] as well as periodic density functional theory (*p*-DFT) methods [28, 29]. In addition, single-point energies calculations were performed at the MP2/6-31+G(d,p) theoretical level, on basis of M06L/6-31+G(d,p) and B3LYP/6-31+G(d,p) optimized structures. The *p*-DFT calculations, as will be elaborated in Section 2.2, were considered in two different conditions; i.e., with and without consideration of dispersion interactions. Figure 2 illustrates the periodic model for β-D-fructofuranose (**F1**).

To account for the bulk solvent effects, MP2/6-31+G(d,p) method was further used in combination with the SMD solvation model [30] developed on basis of the solute electron density and on a continuum model of solvents that was defined by the bulk dielectric constant and atomic tensions. Standard parameters for water solvent as implemented in Gaussian09 software were adopted. In addition, MP2/6-31+G(d,p)//B3LYP/6-31+G(d,p) and MP2/6-31+G(d,p)//M06L/6-31+G(d,p) methods were also employed for calculations of the bulk solvent effects.

2.2. Adsorption of fructose conformers in Sn-BEA Zeolite

As recommended [10-13, 31-34], polymorph A reported by Newsam et al. [35] was used to represent the structure of BEA zeolite. Polymorph A has a tetragonal unit cell with the lattice parameters of a = b = 12.6 Å, c = 26.2 Å. Zeolite BEA has a three-

dimensional pore system with 12-membered rings as the minimum constricting apertures, and as Figure 3 indicates, Sn-BEA zeolite was constructed by situating Sn at one of the T_2 sites, which has been acknowledged to be the most preferential for Sn substitutions [31-34]. The unit cell volume shows an increase due to Sn substitutions, and for Sn-BEA zeolite, the lattice parameters were reported as a = b = 12.657 Å, c = 26.396 Å [33].

Adsorption of the various fructose conformers in Sn-BEA zeolite was investigated with the framework of periodic density functional theory (*p*-DFT), see the model of Sn-BEA zeolite in Figure 3. The Vienna *Ab Initio* Simulation Package (VASP) [28, 29] was employed for such *p*-DFT calculations. The Perdew, Burke and Ernzrhof (PBE) exchange-correlation functional [29] with generalized gradient approximation (GGA) was used, in conjunction with the projected augmented wave (PAW) method to represent electron-ion interactions. All elements were treated with the default PAW pseudopotentials expect Sn, which, as recommended [33, 36], was described by the highest electronic PAW pseudopotential (i.e., Sn_d). The Brillouin zone sampling was restricted to the Γ-point. The energy cutoff was set to 400 eV, and structural optimizations were converged when the forces on each atom of the structures fall below 0.05 eV $Å^{-1}$. The DFT-D2 approach [37] as implemented in VASP5.2 (PBE + U) was employed to account for dispersion interactions, which is the default methodology to treat zeolitic systems and all relating structures and energies were reported at this level unless otherwise specified. Parallel *p*-DFT calculations were also carried out in absence of dispersion interactions, in order to probe their contributions during the adsorption of fructose conformers in Sn-BEA zeolite.

For the various fructose conformers as mentioned earlier, structural optimizations were also performed within the framework of *p*-DFT (Figure 2), and the condition settings were exactly the same as those of adsorption structures in Sn-BEA zeolite. Meanwhile, results thus obtained are necessary for the calculations of adsorption energies. The adsorption energies of fructose conformers in Sn-BEA zeolite were computed to be,

Inclusion of dispersion effects:

$$E_{ad} = E[\text{Sn-BEA-}\mathbf{F_N}(O_i)] - E(\text{Sn-BEA}) - E(\mathbf{F_N}) \quad (1)$$

Absence of dispersion effects:

$$e_{ad} = e[\text{Sn-BEA-}\mathbf{F_N}(O_i)] - e(\text{Sn-BEA}) - e(\mathbf{F_N}) \quad (2)$$

where Sn-BEA, $\mathbf{F_N}$ and Sn-BEA-$\mathbf{F_N}(O_i)$ stand for Sn-BEA, fructose conformers (N = 1, 2, 3, 4, used to discern the various conformers) as well as fructose and Sn-BEA interacted structure with fructose being adsorbed via one of the six O_i atom ($i = 1 \sim 6$), while E and e stand for the energies with and without consideration of dispersion effects, respectively.

Then the contributions of dispersion effects (Δ_{ad}) for each adsorption process in Sn-BEA zeolite were evaluated as,

$$\Delta_{ad} = E_{ad} - e_{ad} \quad (3)$$

3. Results and Discussion

3.1. Gas Phase and Solvent Effects

Fructose conformers in gas phase are first investigated, with aim to comprehend the conformational diversities, relative stabilities and dispersion interactions that are beneficial to understand the subsequent adsorption processes in Sn-BEA zeolite.

Fructose in biochemically relevant polysaccharides exists predominantly as D-furanose while in gas phase predominantly as D-pyranose. In this work, both D-furanose and D-pyranose of fructose have been taken into account, and the lowest-energy conformers of β-,α-D-fructofuranose and β-,α-D-fructopyranose [23, 24], which are designated respectively to be **F1**, **F2** and **F3**, **F4**, have been depicted in Figure 1. D-fructopyranose conformers (**F3** and **F4**) are inclined to construct successive H-bonds ($O_{i+1}H_{i+1}\cdots O_i$ type) that resemble the condition of D-glucopyranose [23, 38], especially in the case of **F3** where the $O_2H_2\cdots O_1$, $O_3H_3\cdots O_2$, $O_4H_4\cdots O_3$ and $O_5H_5\cdots O_4$ H-bonds are optimized at 2.189, 2.275, 2.403 and 2.251 Å, respectively. Successive H-bond networks should be one of the primary driving forces for the conformational preference of D-fructopyranose, in line with the results of D-glucopyranose reported previously [38]. Rather than, interlaced H-bonds play a significant role in D-fructofuranose conformers, such as $O_4H_4\cdots O_2$ (2.097 Å), $O_3H_3\cdots O_6$ (1.939 Å) and $O_1H_1\cdots O_5$ (2.528 Å) in **F1**. Relative stabilities of these conformers increase as **F4** (12.2) < **F2** (4.0) < **F1** (0) << **F3** (-17.6), see Table 1. This is in good agreement with the UV ultrafast laser vaporization and Fourier-transform microwave (FT-MV) spectroscopic observations that free fructose is conformationally locked in the β-D-pyranose form [23]. It should be noted that all structural parameters and relative energies (in parentheses, units in kJ/mol) in gas phase are given at the MP2/6-31+G(d,p) theoretical level, unless otherwise specified.

In addition to the default MP2/6-31+G(d,p) level, other computational methods are used for the investigation of gas-phase fructose conformers (Table 1). As compared to covalent bonds, H-bonds are more sensitive to the choice of computational methods, and the $O_2H_2\cdots O_1$ and $O_5H_5\cdots O_4$ distances in **F3** are 2.276 (0.087) and 2.306 (0.055) Å at HF/6-31+G(d,p) level, 2.190 (0.001) and 2.265 (0.014) Å at B3LYP/6-31+G(d,p)

level, 2.185 (-0.004) and 2.237 (-0.014) Å at M06L/6-31+G(d,p) level, 2.180 (-0.009) and 2.263 (0.012) Å by *p*-DFT calculations with dispersion interactions (PBE + U) and 2.137 (-0.052) and 2.215 (-0.036) Å by *p*-DFT calculations without dispersion interactions. Note that the deviations of H-bond distances from MP2/6-31+G(d,p) data have been given in parentheses. It can be seen that with regard to structural optimizations, density functionals (including *p*-DFT with dispersion interactions; i.e., PBE + U) rather than HF achieve fine agreement with MP2 method. Although the structural parameters of B3LYP density functional are rather close to those of MP2 method, the predicted relative energies for the various fructose conformers may have substantial differences; e.g., a reverse order has been detected for **F1** and **F2** (Table 1); rather than, M06L and *p*-DFT with dispersion interactions have the same trends of relative stabilities as MP2, which explicitly demonstrates the necessity of including dispersion effects for the energy calculations of carbohydrates. This is further corroborated by the HF and *p*-DFT calculations with lack of dispersion interactions that show apparent deviations from MP2 results.

On basis of B3LYP and M06L [26, 27] optimized structures, single-point energy calculations are then carried out at the MP2 theoretical level, and results thus obtained are compared with those directly from MP2 method. It clearly indicates that in addition to the identical changing trends, the exact values of relative energies for the various fructose conformers calculated by MP2/6-31+G(d,p)//B3LYP/6-31+G(d,p) and MP2/6-31+G(d,p)//M06L/6-31+G(d,p) methods are comparable to each other and also very close to those directly from MP2 method (Table 2). Accordingly, B3LYP and other density functionals can be trusted with respect to structural optimizations of

carbohydrates, while it is strongly suggested to include dispersion effects for subsequent energy calculations.

The bulk solvent effects, which are accounted for using the SMD continuum solvation model developed by Truhlar and coworkers [30], have been calculated at the MP2/6-31+G(d,p) theoretical level. Relative energies of the various fructose conformers increase in the order of **F4** (9.4) < **F2** (5.5) < **F1** (0) < **F3** (-13.5) and show the identical changing trends as in gas phase (Table 1), although the exact values may differ somewhat. **F3** still represents the most stable conformer while its preference shows a little reduction due to the inclusion of bulk solvent effects. Relative stabilities of the other two conformers (**F2** and **F4**) have been altered as well. The SMD continuum solvation model is also performed in combination of MP2/6-31+G(d,p)//B3LYP/6-31+G(d,p) and MP2/6-31+G(d,p)//M06L/6-31+G(d,p) methods, and the calculated results are in good agreement with those of MP2/6-31+G(d,p) method (Table 1).

3.2. Adsorption of D-fructofuranose in Sn-BEA Zeolite

Adsorption of the various fructose conformers in Sn-BEA zeolite has been investigated by use of *p*-DFT calculations, with Sn being situated at the T_2 site [31-34]. Figures 4 and 5 indicate that D-fructofuranose conformers (**F1** and **F2**) can be accommodated finely within the large pore of Sn-BEA zeolite. The Sn_2 site displays Lewis acidity towards the incoming D-fructofuranose conformers, and a majority of the O atoms in **F1** and **F2** are accessible to the Sn_2 Lewis acidic site. In general, the Sn_2-O_i distances fall within the range of 2.219 ~ 2.367 Å, in line with the adsorption results of water (Sn_2-O_W: 2.356 Å) and α-D-glucopyranose (Sn_2-O_1: 2.332 Å) [10, 31-34, 39]. Note that O_i (i = 1 ~ 6) refers to the O atoms from fructose conformers. The differences for Sn_2-O_i distances (i = 1 ~ 6) are caused principally by three factors, as steric

hindrance from the adjacent groups of fructofuranose conformers (**F1** and **F2**) as well as H-bonding and vdW interactions with the framework of Sn-BEA zeolite. It has been found that three Sn_2-O_i distances fall out of this range and can be mainly ascribed to steric hindrances from the adjacent groups of fructofuranose conformers (**F1** and **F2**), as Sn_2-O_5 (4.047 Å) for **F1** as well as Sn_2-O_2 (3.043 Å) and Sn_2-O_5 (3.468 Å) for **F2**. Both **F1** and **F2** are in the furanose form, and for D-fructofuranose conformers, each of the two C atoms neighbouring the O_5 atom is linked by a hydroxymethyl group ($CH_{(2)}OH$) that substantially impedes O_5 to approach the Sn_2 Lewis acidic site. For the adsorption of **F2** adsorbed via the O_2 atom, the strong steric hindrances resulting from the posterior O_3H group at the same side of the furanose ring lead to a relatively long distance of Sn_2-O_2, and what aggravates this situation is that the large $C_6H_{(2)}OH$ group is also situated at the same side. Although the steric hindrances from the $C_6H_{(2)}OH$ group are expected to be relieved significantly by rotation, it should correspond to a different conformer of D-fructofuranose and will not be considered herewith. However, these structural obstacles are non-existent in the case of **F1** adsorbed via the O_2 atom, wherein both O_3H and $C_6H_{(2)}OH$ groups fall at the opposite side.

In addition to the construction of direct Sn-O_i bonds, non-covalent interactions (H-bonding and vdW) also exist and play a definite role during the adsorption of D-fructofuranose conformers (**F1** and **F2**) in Sn-BEA zeolite that can be finely simulated by *p*-DFT [10, 15, 33]; e.g., for the adsorption of **F1** via the O_1 atom, the O_2H, O_4H and O_6H groups each form one H-bond with the lattice-O atoms of Sn-BEA zeolite with distances of 1.887, 2.512 and 2.088 Å while C_1H, C_3H and C_6H are closely associated with two, one and one lattice-O atoms with distances of 2.623/2.740, 2.543 and 2.885 Å, respectively. Because of such complicated and forceful non-covalent interactions, the

geometries of D-fructofuranose conformers (**F1** and **F2**) may be distorted to a different extent depending on the strength of non-covalent interactions. As aforementioned, adsorption of **F1** via the O_2 atom experiences relatively mild hindrances and hence the **F1** molecule can approach very close to the framework of Sn-BEA zeolite as evidenced by four short C_1H-O_L distances (2.401, 2.410, 2.491 and 2.679 Å, O_L corresponds to the lattice-O atoms from the six-membered ring where the Sn_2 Lewis acidic site has been situated.). Generally, the closer to the framework of Sn-BEA zeolite, the narrower pore size fructose conformers will be encountered. As a result, the $C_1H_{(2)}OH$ group is seriously rotated and distorted to an appreciable degree, e.g., the $C_3C_2C_1O_1$ and $C_4C_3C_2C_1$ dihedrals are optimized at 176.05°, 160.47° in the isolated **F1** molecule and -94.31° and 145.03° when adsorbed in Sn-BEA zeolite, respectively. Instead, adsorption of **F2** via the O_2 atom causes very slight structural alterations and the **F2** geometries before and after adsorption can almost be superimposed with each other.

Figure 6 shows that the adsorption energies of D-fructofuranose conformers (**F1** and **F2**) on the Sn_2 site of Sn-BEA zeolite respectively fall within the ranges of -99.5 ~ -157.2 and -88.0 ~ -161.5 kJ/mol for **F1** and **F2**, which are in line with those of α-D-glucopyranose [10] but obviously larger than those of small molecules (e.g., H_2O and NH_3) [31-34, 39]. As will be elaborated subsequently [15-17, 40-43], dispersion interactions contribute more significantly to the adsorption energies for guest molecules with larger sizes. With regard to each fructose conformer, the adsorption energies can differ substantially for the various O sites, due to the variations of Sn_2-O_i bond strengths, H-bonding and vdW interactions as discussed earlier. The largest adsorption energies for **F1** and **F2** in Sn-BEA zeolite correspond to the O_4 and O_6 sites, respectively.

3.3. Adsorption of D-fructopyranose in Sn-BEA Zeolite

Figures 7 and 8 display the adsorption configurations of D-fructopyranose conformers (**F3** and **F4**) via the various O sites on the Sn_2 site of Sn-BEA zeolite, and it can be seen that although with a larger ring than D-fructofuranose conformers (**F1** and **F2**), D-fructopyranose conformers (**F3** and **F4**) can also be well held within the mesoporous BEA zeolite. For each D-fructopyranose conformer, five out of the six O sites construct direct Sn-O_i bonds with Sn-BEA zeolite, and the Sn-O_i bonds differ in the various adsorption configurations that change with the range of 2.217 ~ 2.376 Å, consistent with the adsorption results of water and α-D-glucopyranose [10] as well as D-fructofuranose discussed above. The Sn-O_i bond distances are averaged respectively at 2.292, 2.284, 2.314 and 2.277 Å for **F1**, **F2**, **F3** and **F4**, which clearly demonstrates that on the average, the Sn-O_i interaction strengths are almost unaffected by the choice of different rings (furanose for **F1** and **F2** while pyranose for **F3** and **F4**); nonetheless, the Sn-O_i interaction strengths are sensitive to the various O_i sites and various fructose conformers (Figures 4, 5, 7 and 8), as a combined effect of steric hindrances from the adjacent groups as well as H-bonding and vdW interactions; e.g., adsorption of **F3** and **F4** via the O_1 atom each creates three H-bonds with the lattice-O atoms of Sn-BEA zeolite, respectively as O_2H: 1.762 Å, O_4H: 2.827 Å, O_5H: 1.891 Å and O_2H: 1.981 Å, O_3H: 2.271 Å, O_5H: 2.681 Å. These H-bonds, along with vdW interactions from CH groups, are quite different from each other and also from the condition of D-fructofuranose conformers (**F1** and **F2**) discussed above. As indicated in Figure 1, the O_1 sites in all fructose conformers presently investigated (**F1**, **F2**, **F3** and **F4**) are rather flexible and therefore correspond to the less steric hindrances than in α-D-glucopyranose (Sn_2-O_1: 2.332 Å) [10]. As a matter of fact, the most conspicuous difference between D-fructofuranose and D-fructopyranose during the interaction with

Sn-BEA zeolite lies in their O_5 and O_6 sites. The O_6 atoms in **F3** and **F4** are within the pyranose rings that remain structurally rigid, and so relatively the large steric hindrances will be encountered from adjacent groups during the interaction with the Sn_2 Lewis acidic site. The Sn-O_R distances (O_R refers to O atoms from the rings) increase as α-D-glucopyranose (2.450 Å, O_5) [10] < **F4** (3.160 Å, O_6) < **F2** (3.468 Å, O_5) < **F3** (3.576 Å, O_6) < **F1** (4.047 Å, O_5), and such differences are mainly caused by the variation of steric obstacles, which are minimal with respect to α-D-glucopyranose [8, 10]. Approach of α-D-glucopyranose to the Sn_2 Lewis acidic site is hampered only by the O_1H group that is counteracted largely by formation of one strong H-bond with lattice-O atoms (1.810 Å) [10].

As indicated in Figure 6, the adsorption energies of **F3** and **F4** on the Sn_2 site of Sn-BEA zeolite are calculated to vary respectively within the ranges of -101.7 ~ -136.1 and -73.3 ~ -141.2 kJ/mol. In line with the results of D-fructofuranose conformers, the adsorption energies of D-fructopyranose conformers corresponding to the various O sites may have significant differences. Interactions of the O_3 and O_4 sites with Sn-BEA zeolite result in the largest adsorption energies for **F3** and **F4**, respectively. The interaction strengths of the various fructose conformers with Sn-BEA zeolite may have noticeable differences, and the adsorption energies averaged over the six O sites increase as **F4** (-112.9) < **F2** (-114.5) < **F3** (-119.6) < **F1** (-126.7). It is assumed that for each fructose conformer, the adsorption configuration is presented as the optimal structure that corresponds to the largest adsorption energy. The maximal adsorption energies of **F1**, **F2**, **F3** and **F4** within Sn-BEA zeolite are equal to -157.2 (O_4), -161.5 (O_6), -136.1 (O_3) and -141.2 (O_4) kJ/mol, respectively. Accordingly, the various fructose conformers within Sn-BEA zeolite result in an appreciable difference in their

adsorption energies, and D-fructofuranose conformers are significantly preferred over D-fructopyranose conformers during the interaction with Sn-BEA zeolite that may fundamentally alter the conformational distribution of gas phase.

3.4. Relative Stability and Dispersion Interaction in Sn-BEA Zeolite

Relative energies of the various fructose conformers (**F1**, **F2**, **F3** and **F4**) in Sn-BEA zeolite have been calculated and listed in Table 2. It can be seen that the relative stabilities for one fructose conformer are strongly dependent on the adsorption O sites ($O_1 \sim O_6$); e.g., the relative stabilities of **F1** in Sn-BEA zeolite increase in the order of 57.7 (O_5) < 43.7 (O_2) < 32.9 (O_1) < 30.9 (O_6) < 18.0 (O_3) < 0 (O_4), which is consistent with the changing trends of adsorption energies. As discussed earlier, the adsorption configuration for each fructose conformer should be presented as the optimal structure characterized by the largest adsorption energy. With consideration of the most stable configurations, the relative stabilities for the various fructose conformers adsorbed within Sn-BEA zeolite rank as **F4** (23.1) ≤ **F3** (23.0) < **F1** (0) < **F2** (-1.1), which is totally different from the condition of gas phase (**F4** < **F2** < **F1** < **F3**) as demonstrated in Section 3.1. **F3** represents the predominant conformer for fructose in gas phase, while it is the least preferred when adsorbed within Sn-BEA zeolite. Rather than, the prior choice of Sn-BEA zeolite is conformers with the furanose form (**F1** and **F2**), which coincides perfectly with the fact that fructose in biochemically relevant polysaccharides exists predominantly in the furanose form. Owing to the pronounced differences of their relative stabilities and further conformational distributions, the mechanistic studies with catalysis by Sn-BEA zeolite can be confidently based on the furanose form that has been widely used in the previous works [8, 10-13].

As stated in Section 3.1, dispersion effects play a role in the case of gas-phase fructose conformers and alter their relative stabilities somewhat. According to the *p*-DFT calculated results (Table 1), relative stabilities in gas phase increase in the order of **F4** (7.1) < **F2** (3.1) < **F1** (0) < **F3** (-7.4) according to the *p*-DFT calculations with dispersion interactions while of **F4** (10.4) < **F1** (0) < **F2** (-1.3) < **F3** (-13.0) according to the *p*-DFT calculations without dispersion interactions, respectively. That is, dispersion interactions alter the relative stabilities of gas-phase fructose conformers whereas the alteration maximum is not more than 5.6 kJ/mol. However, it is expected that dispersion effects will exert a considerably larger influence during the interaction with Sn-BEA zeolite.

Figures 4, 5, 7 and 8 indicate that perturbations to the Sn-O_i distances due to lack of dispersion interactions are generally small. The more obvious perturbations generally correspond to those without the formation of direct Sn-O bonds; e.g., 3.160 vs. 3.405 Å for **F4** adsorption via the O_6 site. For the direct Sn-O bonds, some are elongated (e.g., 2.253 vs. 2.279 Å for **F1** adsorption via the O_3 site) while the others are shortened (e.g., 2.367 vs. 2.253 Å for **F1** adsorption via the O_2 site), suggesting that a portion of Sn-O_i interactions may be corroborated due to the absence of dispersion interactions.

Although widely used, density functional theory (DFT) methods are known to be insufficient to treat dispersion interactions, and hence a number of computational schemes (e.g., hybrid MP2:DFT and presently used PBE + U) have been proposed that properly account for such interactions [15-17, 19, 20, 40-43]. The contributions of dispersion effects for all relating adsorption structures shown in Figures 4, 5, 7 and 8 are evaluated by use of Eq. 3 given in Section 2.2. Table 3 indicates that for each fructose conformer, the contributions of dispersion effects may differ significantly for the

various adsorption sites (O_1 ~ O_6), which is similar to the condition of adsorption energies (Figure 6). In addition, no clear correlation has been detected between the adsorption energies and dispersion interactions; e.g., for **F1**, the O_4 and O_5 sites correspond to the largest and smallest adsorption energies while the maximal and minimal dispersion interactions are resulted from the O_3 and O_6 sites, respectively. For every fructose conformer, dispersion interactions are averaged for the various O sites (O_1 ~ O_6) that amount to -123.8, -123.4, -125.6 and -127.5 kJ/mol for **F1**, **F2**, **F3** and **F4**, respectively. Dispersion interactions during the adsorption of NH_3, CH_3NH_2, $(CH_3)_2NH$ and $(CH_3)_3N$ in H-MOR zeolite have been evaluated by Soto and collaborators [43] that are the most significant in the case of $(CH_3)_3N$ (-92 kJ/mol according to B3LYP-D3:B3LYP scheme). Fructose has an obviously larger molecular size and hence dispersion interactions are expected play a larger role during the adsorption in zeolites. As corroborated by Cheng et al. [15], dispersion interactions account for -127.5 kJ/mol for the adsorption of **F1** via the O_1 site in H-ZSM-5 zeolite that are in line with the present results of Sn-BEA zeolite. However, differences can still be detected between the works of Cheng et al. [15] and ours that can be ascribed to the pore structures (ZSM-5 vs. BEA), type of substitutions ([Al, H] vs. Sn) as well as sensitivity of O sites (only the O_1 site considered in Ref. [15] vs. the average for six O sites in this work). Meanwhile, it can be seen that the averaging dispersion interactions are close for all fructose conformers, and those of D-fructopyranose rather than D-fructofuranose seem to be a bit larger. Dispersion effects play an apparently larger role when adsorbed in Sn-BEA zeolite than in gas phase, where the alteration by dispersion interactions accounts for not more than 5.6 kJ/mol.

4. Conclusions

Biomass energy represents a potential alternative for petroleum resources that are to be exhausted within the few decades. Fructose has been regarded as one of the key intermediate products for the transformation of cellulosic biomass to downstream products. Sn-BEA zeolite displays unprecedented catalytic activity for the isomerization of glucose (monomer of cellulose) to fructose. In this work, *ab initio* and density functional theory calculations based on cluster and periodic models have been performed to address the gas-phase fructose conformations, their adsorption behaviors in Sn-BEA zeolite and the contributions of dispersion effects. The main findings are summarized as follows:

In gas phase, the relative stabilities of the various fructose conformers increase as **F4** (12.2 kJ/mol) < **F2** (4.0 kJ/mol) < **F1** (0 kJ/mol) < **F3** (-17.6 kJ/mol), where the D-furanose form (**F1** and **F2**) that predominates in biochemically relevant polysaccharides is strongly disfavoured. B3LYP and other density functionals (including M06L and *p*-DFT) rather than HF are sufficient for structural optimizations of carbohydrates, while it is strongly suggested to include dispersion interactions for energy calculations. The bulk solvent effects calculated by the SMD continuum solvation model indicate an identical changing trend of relative stabilities as in gas phase, while the exact values may differ with the preference of **F3** decreasing somewhat.

The various fructose conformers, whether in the D-furanose or D-pyranose form, can be finely accommodated finely within the nanoporous Sn-BEA zeolite. Fructose conformers can via the various O sites approach the Sn_2 site that shows Lewis acidity, resulting in Sn_2-O_i bond distances within the range of 2.217 ~ 2.376 Å that are consistent with the adsorption results of α-D-glucopyranose and water. On the average,

the Sn-O_i interaction strengths are almost unaffected by the choice of different rings (furanose or pyranose); nonetheless, the Sn_2-O_i distances (i = 1 ~ 6) show differences for the various fructose conformers and various O sites of these conformers, which are caused mainly by steric hindrances from the adjacent groups as well as H-bonding and vdW interactions with the framework of Sn-BEA zeolite. 5 out of 24 adsorption configurations are characterized by long Sn_2-O_i distances (> 3.0 Å), mainly due to steric hindrances from the adjacent groups as evidenced by structural analyses (4 cases correspond to the cyclic-O atoms). Non-covalent interactions (H-bonding and vdW) exist between the fructose conformers and framework of Sn-BEA zeolite, which may cause the geometries of fructose conformers to be distorted to a certain extent depending mainly on the strength of non-covalent interactions.

The adsorption energies of **F1**, **F2**, **F3** and **F4** on the Sn_2 site of Sn-BEA zeolite fall within the ranges of -99.5 ~ -157.2, -88.0 ~ -161.5, -101.7 ~ -136.1 and -73.3 ~ -141.2 kJ/mol, respectively. The largest adsorption energies for these fructose conformers correspond to the O_4, O_6, O_3 and O_4 sites, respectively. With regard to each fructose conformer, the adsorption energies can differ substantially for the various O sites, mainly due to the variation of Sn_2-O_i bond strengths, H-bonding and vdW interactions. The adsorption configuration of each fructose conformer is assumed to be the structure with the largest adsorption energy, and D-fructofuranose conformers are significantly preferred over D-fructopyranose conformers during the interaction with Sn-BEA zeolite that may fundamentally alter the conformational preference and distribution of gas phase. This is corroborated the calculated relative stabilities that rank as **F4** (23.1 kJ/mol) ≤ **F3** (23.0 kJ/mol) < **F1** (0 kJ/mol) < **F2** (-1.1 kJ/mol). Accordingly, the D-furanose form that predominates in biochemically relevant polysaccharides exists favorably in

Sn-BEA zeolite, which can confidently be used for mechanistic studies as found in all previous works.

Dispersion interactions exist in the case of gas-phase fructose conformers and can alter their relative stabilities at a maximum of 5.6 kJ/mol. However, dispersion effects play a considerably larger role during the interaction with Sn-BEA zeolite that, averaged over the various O sites, are equal to -123.8, -123.4, -125.6 and -127.5 kJ/mol for **F1**, **F2**, **F3** and **F4**, respectively. The average dispersion interactions are close for all fructose conformers, and those of D-fructopyranose rather than D-fructofuranose are a bit larger. For each fructose conformer, the contributions of dispersion effects may differ significantly for the various O sites.

Acknowledgments

This work was sponsored by the National Natural Science Foundation of China (21473137) and Fourth Excellent Talents Program of Higher Education in Chongqing (2014-03) and Fundamental Research Funds for the Central Colleges (SWU113049 and XDJK2014C106).

References and Notes

1. Zhou, C. H.; Xia, X.; Lin, C. X.; Tong, D. S.; Beltramini, J. Catalytic Conversion of Lignocellulosic Biomass to Fine Chemicals and Fuels. *Chem. Soc. Rev.* **2011**, *40*, 5588-5617.

2. Arvela, P. M.; Simakova, I. L.; Salmi, T.; Murzin, D. Y. Production of Lactic Acid/Lactates from Biomass and Their Catalytic Transformations to Commodities. *Chem. Rev.* **2014**, *114*, 1909-1971.

3. Yang, G.; Pidko, E. A.; Hensen, E. J. M. Mechanism of Brønsted Acid Catalyzed Conversion of Carbohydrates. *J. Catal.* **2012**, *295*, 122-132.

4. Moliner, M.; Román-Leshkov, Y.; Davis, M. E. Tin-containing Zeolites are Highly Active Catalysts for the Isomerization of Glucose in Water. *Proc. Natl. Acd. Sci. USA* **2010**, *107*, 6164-6168.

5. Pidko, E. A.; Degirmenci, V.; van Santen, R. A.; Hensen, E. J. M. Glucose Activation by Transient Cr^{2+} Dimer. *Angew. Chem. Int. Ed.* **2010**, *49*, 2530-2534.

6. Assary, R. S.; Redfern, P. C.; Hammond, J. R.; Greeley, J.; Curtiss, L. A. Computational Studies of the Thermochemistry for Conversion of Glucose to Levulinic Acid. *J. Phys. Chem. B* **2010**, *114*, 9002-9009.

7. Assary, R. S.; Redfern, P. C.; Hammond, J. R.; Greeley, J.; Curtiss, L. A. Mechanistic Insights into the Decomposition of Fructose to Hydroxy Methyl Furfural in Neutral and Acidic Environments Using High-Level Quantum Chemical Methods. *J. Phys. Chem. B* **2010**, *115*, 4341-4349.

8. Bermejo-Deval, R.; et al. Metalloenzyme-like catalyzed isomerizations of sugars by Lewis acid zeolites. *Proc. Natl. Acd. Sci. USA* **2012**, *109*, 9727-9732.

9. Qian, X. H.; Wei, X. F. Glucose Isomerization to Fructose from ab Initio Molecular

Dynamics Simulations. *J. Phys. Chem. B* **2012**, *116*, 10898-10904.

10. Yang, G.; Pidko, E. A.; Hensen, E. J. M. The Mechanism of Glucose Isomerization to Fructose over Sn-BEA Zeolite: A Periodic Density Functional Theory Study. *ChemSusChem* **2013**, *6*, 1688-1696.

11. Rai, N.; Caratzoulas, S.; Vlachos, D. G. Role of Silanol Group in Sn-Beta Zeolite for Glucose Isomerization and Epimerization Reactions. *ACS Catal.* **2013**, *3*, 2294-2298.

12. Li, Y. P.; Head-Gordon, M.; Bell, A. T. Analysis of the Reaction Mechanism and Catalytic Activity of Metal-Substituted Beta Zeolite for the Isomerization of Glucose to Fructose. *ACS Catal.* **2014**, *4*, 1537-1545.

13. Christianson, J. R.; Caratzoulas, S.; Vlachos, D. G. Computational Insight into the Effect of Sn-Beta Na Exchange and Solvent on Glucose Isomerization and Epimerization, *ACS Catal.* **2015**, *5*, 9, 5256-5263.

14. Caratzoulas, S.; Vlachos, D. G. Converting Fructose to 5-Hydroxymethylfurfural: A Quantum Mechanics/Molecular Mechanics Study of the Mechanism and Energetics. *Carbohydrate Res.* **2011**, *346*, 664-672.

15. Cheng, L.; Curtiss, L. A.; Assary, R. S.; Greeley, J.; Kerber, T.; Sauer, J. Adsorption and Diffusion of Fructose in Zeolite HZSM-5: Selection of Models and Methods for Computational Studies. *J. Phys. Chem. C* **2011**, *115*, 21785-21–21790.

16. de Moor, B. A.; Reyniers, M. F.; Sierka, M. Sauer, J. Physisorption and Chemisorption of Hydrocarbons in H-FAU Using QM-Pot(MP2//B3LYP) Calculations. *J. Phys. Chem. C* **2008**, *112*, 11796-11812.

17. Svelle, S.; Tuma, C.; Rozanska, X.; Kerber, T.; Sauer, J. Quantum Chemical Modeling of Zeolite-Catalyzed Methylation Reactions: Toward Chemical Accuracy for Barriers. *J. Am. Chem. Soc.* **2009**, *131*, 816-825.

18. Vandichel, M.; Lesthaeghe, D.; van der Mynsbrugge, J.; Waroquier, M.; van Speybroeck, V. Assembly of Cyclic Hydrocarbons from Ethene and Propene in Acid Zeolite Catalysis to Produce Active Catalytic Sites for MTO Conversion**.** *J. Catal.* **2011**, *271*, 67-78.

19. Yang, G., Zhou, L. J. A DFT Study on Direct Benzene Hydroxylation Catalyzed by Framework Fe and Al Sites in Zeolites. *Catal. Sci. Technol.* **2014**, *4*, 2490-2493.

20. Yang, G.; Zhou, L. J. Zwitterionic versus Canonical Amino Acids over the Various Defects in Zeolites: A two-layer ONIOM Calculation. *Sci. Rep.* **2014**, *4*, 6594.

21. Xin, H. C.; Li, X. P.; Fang, Y.; Yi, X. F.; Hu, W. H.; Chu, Y. Y.; Zhang, F.; Zheng, A. M.; Zhang, H. P.; Li, X. B. Catalytic Dehydration of Ethanol over Post-treated ZSM-5 Zeolites. *J. Catal.* **2014**, *312*, 204-215.

22. Wang, C.; Chu, Y. Y.; Zheng, A. M.; Xu, J.; Wang, Q.; Gao, P.; Qi, G. D.; Gong, Y. J.; Deng, F.New Insight into the Hydrocarbon-Pool Chemistry of the Methanol-to-Olefins Conversion over Zeolite H-ZSM-5 from GC-MS, Solid-State NMR Spectroscopy, and DFT Calculations. *Chem. Eur. J.* **2014**, *20*, 12432-12443.

23. Cocinero, E. J.; Lesarri, A.; Écija, P.; Cimas, Á; Davis, B. G.; Basterretxea, F. J.; Fernández, J. A.; Castaño, F. Free Fructose Is Conformationally Locked. *J. Am. Chem. Soc.* **2013**, *135*, 2845-2852.

24. Chung-Phillips, A.; Chen, Y. Y. An ab Initio Study of Fructose in the Gas Phase. *J. Phys. Chem. A* **1999**, *103*, 953-964.

25. Frisch, M. J.; Trucks, G. W.; Schlegel, H. B.; Scuseria, G. E.; Robb, M. A. ; et al. *Gaussian 09, Revision A.9*, Gaussian, Inc.: Wallingford CT, **2013**.

26. Zhao, Y.; Truhlar, D. G. A New Local Density Functional for Main-group Thermochemistry, Transition Metal Bonding, Thermochemical Kinetics, and

Noncovalent Interactions. *J. Chem. Phys*. **2006**, *125*, no. 194101.

27. Zhao, Y.; Truhlar, D. G. The M06 Suite of Density Functionals for Main Group Thermochemistry, Thermochemical Kinetics, Noncovalent Interactions, Excited States, and Transition Elements: Two New Functionals and Systematic Testing of Four M06-class Functionals and 12 Other Functionals. *Theor. Chem. Acc*. **2008**, *120*, 215-241.

28. Kresse, G.; Furthmuller, J. Efficiency of ab-initio Total Energy Calculations for Metals and Semiconductors Using a Plane-wave Basis Set. *Comput. Mater. Sci*. **1996**, *6*, 15-50.

29. Perdew, J. P.; Burke, K.; Ernzerhof, M. Generalized Gradient Approximation Made Simple. *Phys. Rev. Lett.* **1996**, *77*, 3865-3868.

30. Marenich, A. V.; Cramer, C. J.; Truhlar, D. G. Universal Solvation Model Based on Solute Electron Density and a Continuum Model of the Solvent Defined by the Bulk Dielectric Constant and Atomic Surface Tensions. *J. Phys. Chem. B* **2009**, *113*, 6378-6396.

31. Shetty, S.; Pal, S.; Kanhere, D. G.; Goursot, A. Structural, Electronic, and Bonding Properties of Zeolite Sn-Beta: A Periodic Density Functional Theory Study. *Chem. Eur. J.* **2006**, *12*, 518-523.

32. Shetty, S.; Kulkarni, B. S.; Kanhere, D. G.; Goursot, A.; Pal, S. A Comparative Study of Structural, Acidic and Hydrophilic Properties of Sn-BEA with Ti-BEA Using Periodic Density Functional Theory. *J. Phys. Chem. B* **2008**, *112*, 2573-2579.

33. Yang, G.; Pidko, E. A.; Hensen, E. J. M. Structure, Stability, and Lewis Acidity of Mono and Double Ti, Zr, and Sn Framework Substitutions in BEA Zeolites: A Periodic Density Functional Theory Study. *J. Phys. Chem. C* **2013**, 117, 3976-3986.

34. Montejo-Valencia, B. D.; Curet-Arana, M. C. DFT Study of the Lewis Acidities and Relative Hydrothermal Stabilities of BEC and BEA Zeolites Substituted with Ti, Sn, and Ge. *J. Phys. Chem. C* **2015**, *119*, 4148-4157.

35. Newsam, J. M.; Treacy, M. M. J.; Koestsier, W. T.; de Gruyter, C. B. Structural Characterization of Zeolite Beta. *Proc. R. Soc. London Ser. A* **1988**, *420*, 375-405.

36. Jain, A.; Hautier, G.; Moore, C. J.; Ong, S. P.; Ficher, C. C.; Mueller, T.; Persson, K. A.; Ceder, G. A High-throughput Infrastructure for Density Functional Theory Calculations. *Comput. Mater. Sci.* **2011**, *50*, 2295-2310.

37. Grimme, S. Semiempirical GGA-type Density Functional Constructed with a Long-range Dispersion Correction. *J. Comput. Chem.* **2006**, *27*, 1787-1799.

38. Alonso, J. L.; Lozoya, M. A.; Peňa, I.; López, J. C.; Cabezas, C.; Mata, S.; Blanco, S. The Conformational Behaviour of Free D-glucose - At Last. *Chem. Sci.* **2014**, *5*, 515-522.

39. Yang, G.; Zhou, L. J.; Han, X. W. Lewis and Brönsted Acidic Sites in M^{4+}-doped Zeolites (M = Ti, Zr, Ge, Sn, Pb) as Well as Interactions with Probe Molecules: A DFT Study. *J. Mol. Catal. A: Chemical* **2012**, *363-364*, 371-379.

40. Hansen, N. Kerber, T.; Sauer, J. Bell, A. T.; Keil, F. J. Quantum Chemical Modeling of Benzene Ethylation over H-ZSM-5 Approaching Chemical Accuracy: A Hybrid MP2:DFT Study. *J. Am. Chem. Soc.* **2010**, *132*, 11525-11538.

41. Nguyen, C. M.; de Moor, B. A.; Reyniers, M. F. Marin, G. B. Physisorption and Chemisorption of Linear Alkenes in Zeolites: A Combined QM-Pot(MP2//B3LYP: GULP)-Statistical Thermodynamics Study. *J. Phys. Chem. C* **2011**, *115*, 23831-23847.

42. Yang, G.; Zhou, L. J.; Liu, X. C.; Han, X. W.; Bao, X. H. Adsorption, Reduction and Storage of Hydrogen within ZSM-5 Zeolite Exchanged with Various Ions: A Comparative Theoretical Study. *Micropor. Mesopor. Mater.* **2012**, *161*, 168-178.

43. Soto, L. D.; Sierraalta, A.; Añez, R. Nascimento, M. A. C. Theoretical Study of the Adsorption of Alkylamines in H‑Mordenite: The Role of Noncovalent Interactions. *J. Phys. Chem. C* **2015**, *119*, 8112-8123.

Table 1. Relative energies (kJ/mol) of different fructose conformers in gas phase that have been calculated at the various levels of theory [a]

	F1	**F2**	**F3**	**F4**
MP2/6-31+G(d,p) [b]	0 (0)	4.0 (5.5)	-17.6 (-13.5)	12.2 (9.4)
HF/6-31+G(d,p)	0	-3.9	-20.5	10.5
B3LYP/6-31+G(d,p)	0	-1.9	-15.9	10.5
M06L/6-31+G(d,p)	0	0.9	-19.1	5.0
p-DFT (PBE + U) [c]	0 (0)	3.1 (-1.3)	-7.4 (-13.0)	7.1 (10.4)
MP2/6-31+G(d,p)//	0	4.2	-17.4	12.2
B3LYP/6-31+G(d,p) [b]	(0)	(5.5)	(-11.4)	(11.8)
MP2/6-31+G(d,p)//	0	4.2	-17.7	12.6
M06L/6-31+G(d,p) [b]	(0)	(4.2)	(-12.9)	(10.5)

[a] **F1** as energy benchmark;

[b] Data of SMD solvation model in parentheses;

[c] Data in absence of dispersion interactions are shown in parentheses.

Table 2. Relative energies (kJ/mol) of different adsorption configurations for the various fructose conformers in Sn-BEA zeolite

	F1 [a]	**F2**	**F3**	**F4**
O_1	32.9	46.0	48.1	66.0
O_2	43.7	52.9	29.0	48.0
O_3	18.0	56.9	13.7	25.9
O_4	0	72.3	37.1	23.1
O_5	57.7	48.2	23.0	90.9
O_6	30.9	-1.1	30.2	54.5

[a] Adsorption structure of **F1** via the O_4 site as energy benchmark.

Table 3. Contributions of dispersion effects (kJ/mol) for the adsorption of the various fructose conformers in Sn-BEA zeolite

	F1	**F2**	**F3**	**F4**
O_1	-125.7	-123.1	-141.9	-134.4
O_2	-149.5	-107.6	-115.1	-131.0
O_3	-130.4	-120.3	-111.9	-122.0
O_4	-110.7	-139.1	-144.7	-128.2
O_5	-117.9	-116.7	-128.8	-144.3
O_6	-108.6	-133.6	-111.1	-105.1
Average [a]	-123.8	-123.4	-125.6	-127.5

[a] Dispersion interactions averaged over the six O sites of fructose conformers.

Figure captions:

Figure 1. Optimized structures of β-D-fructofuranose (**F1**), α-D-fructofuranose (**F2**), β-D-fructopyranose (**F3**) and α-D-fructopyranose (**F4**). H-bonds are marked in blue dashed lines.

Figure 2. Periodic model to simulate β-D-fructofuranose (**F1**). Cell parameters a = b = c = 20.0 Å with **F1** being at the center.

Figure 3. Periodic model of Sn-BEA zeolite with Sn being situated at the T_2 site.

Figure 4. Adsorption configurations of β-D-fructofuranose (**F1**) via the various O sites on the Sn_2 site of Sn-BEA zeolite. Distances (Å) in parentheses are in absence of dispersion effects. H-bonds with the lattice O atoms of Sn-BEA zeolite are marked in blue dashed lines.

Figure 5. Adsorption configurations of α-D-fructofuranose (**F2**) via the various O sites on the Sn_2 site of Sn-BEA zeolite. Distances (Å) in parentheses are in absence of dispersion effects. H-bonds with the lattice O atoms of Sn-BEA zeolite are marked in blue dashed lines.

Figure 6. Adsorption energies of different fructose conformers on the Sn_2 site of Sn-BEA zeolite.

Figure 7. Adsorption configurations of β-D-fructopyranose (**F3**) via the various O sites on the Sn_2 site of Sn-BEA zeolite. Distances (Å) in parentheses are in absence of dispersion effects. H-bonds with the lattice O atoms of Sn-BEA zeolite are marked in blue dashed lines.

Figure 8. Adsorption configurations of α-D-fructopyranose (**F4**) via the various O sites on the Sn_2 site of Sn-BEA zeolite. Distances (Å) in parentheses are in absence of

dispersion effects. H-bonds with the lattice O atoms of Sn-BEA zeolite are marked in blue dashed lines.

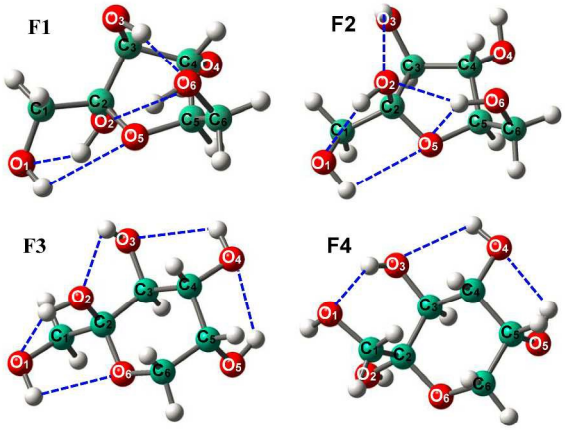

Figure 1

297x420mm (300 x 300 DPI)

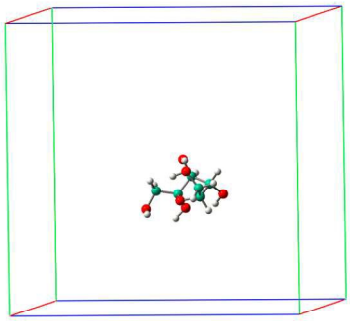

Figure 2

297x420mm (300 x 300 DPI)

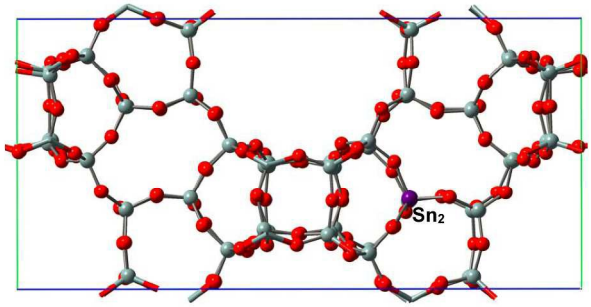

Figure 3

297x420mm (300 x 300 DPI)

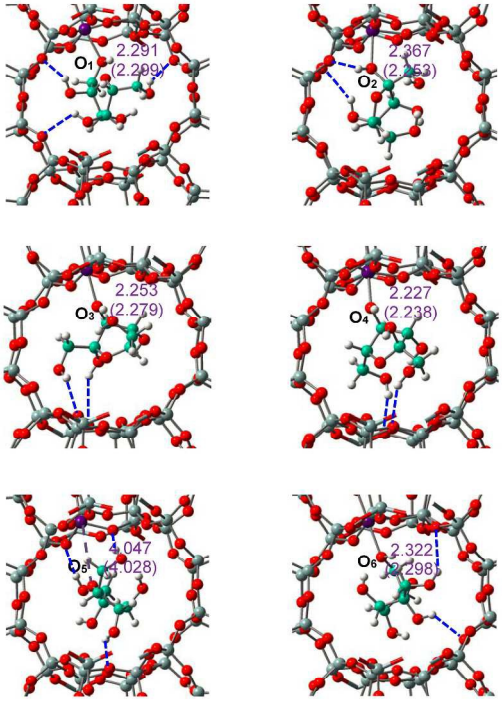

Figure 4

297x420mm (300 x 300 DPI)

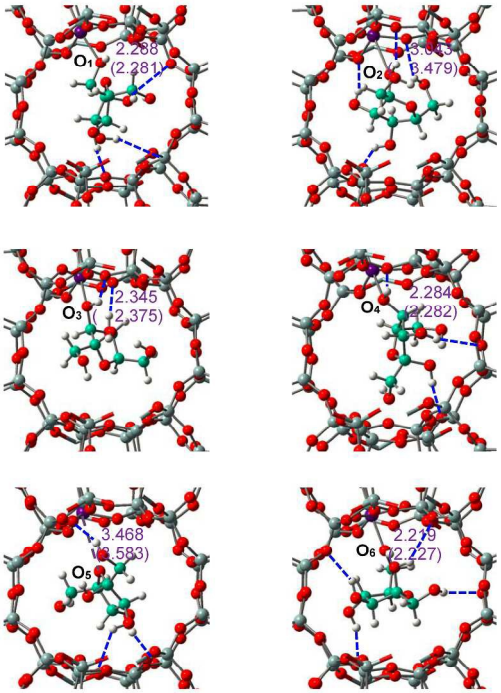

Figure 5

297x420mm (300 x 300 DPI)

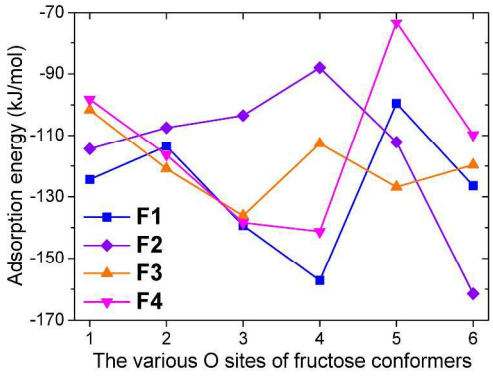

Figure 6

297x420mm (300 x 300 DPI)

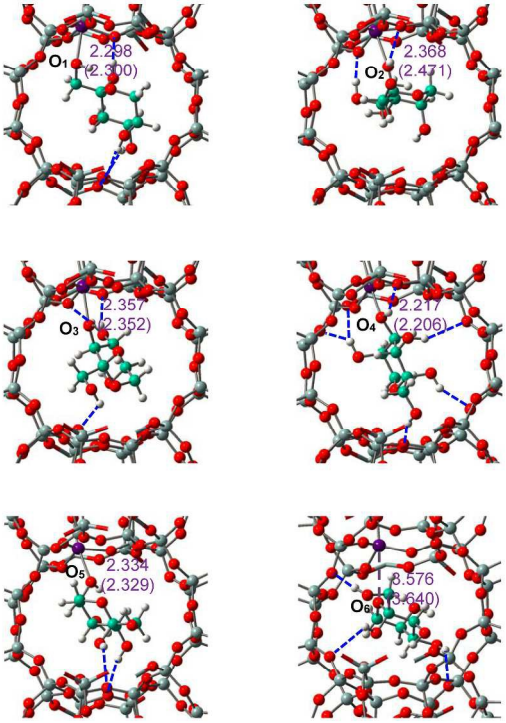

Figure 7

297x420mm (300 x 300 DPI)

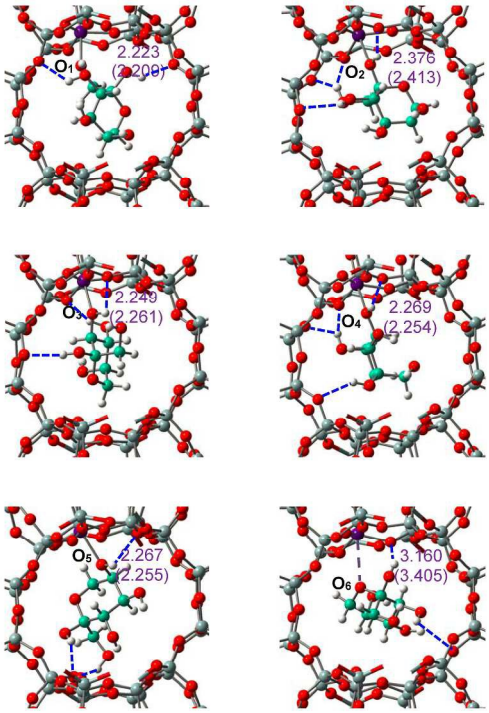

Figure 8

297x420mm (300 x 300 DPI)

Table of contents entry (Graphic)

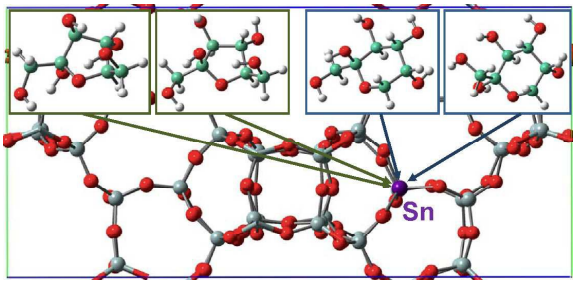

Text

Sn-BEA zeolite selects fructose conformers from biochemically relevant polysaccharides rather than gas phase, and dispersion effects contribute significantly during interactions.